Proceedings of OMAE 2009
28th International Conference on Ocean, Offshore and Arctic Engineering
May 31–June 5, 2009, Honolulu, Hawaii

OMAE2009-79595

Numerical Simulation of Surface Waves Generated by a Subaerial Landslide at Lituya Bay, Alaska

Debashis Basu, Steve Green, Kaushik Das, Ron Janetzke, John Stamatakos
Southwest Research Institute®
6220 Culebra Road, San Antonio, TX 78238, USA

ABSTRACT

This paper presents preliminary results of a computational study conducted to analyze the impulse waves generated by the subaerial landslide at Lituya Bay, Alaska. The volume of fluid (VOF) method is used to track the free surface and shoreline movements. The Renormalization Group (RNG) turbulence model and Detached Eddy Simulation (DES) multiscale model were used to simulate turbulence dissipation. The subaerial landslide is simulated using a sliding mass. Results from the two-dimensional (2-D) simulations are compared with results from a scaled-down experiment. The experiment is carried out at a 1:675 scale. In the experimental setup, the subaerial rockslide impact into the Gilbert Inlet, wave generation, propagation, and runup on the headland slope are considered in a geometrically undistorted Froude similarity model. The rockslide is simulated by a granular material driven by a pneumatic acceleration mechanism so that the impact characteristics can be controlled. Simulations are performed for different values of the landslide density to estimate the influence of slide deformation on the generated tsunami characteristics. Simulated results show the complex flow patterns in terms of the velocity field, shoreline evolution, and free surface profiles. The predicted wave runup height is in close agreement with both the observed wave runup height and that obtained from the scaled-down experimental model.

1. INTRODUCTION

Tsunamis are typically generated by co-seismic sea bottom displacement due to earthquakes. However, submarine or subaerial landslides can trigger devastating tsunamis. Underwater landslides represent the second most important source of tsunami generation and create more devastating tsunamis than co-seismic tsunami sources of moderate strength. These types of tsunamis can produce large runup heights that flood the coast. Landslide-generated tsunamis are triggered by the impact of a sub-aerial fast landslide against the otherwise undisturbed water body. Subaerial landslides can attain large velocities before transferring energy to water waves [1]. The impact of these subaerial landslides with water bodies can lead to significant damages along the shore line.

Submarine landslides are also one of the main mechanisms through which sediments are transferred across the continental slope to the deep ocean [2]. They are widespread on submarine slopes, particularly in areas where fine-grained sediments are present. Tsunami hazards posed by submarine landslides depend on the landslide scale, location, type, and process. Even small submarine landslides can be dangerous when they occur in coastal areas. Examples include the 1996 Finneidfjord slide [3] and the 1929 Grand Banks earthquake that resulted in submarine landslides, turbidity current, and a tsunami that caused significant casualties [2, 4, 5].

Although the generation and propagation of earthquake-generated tsunamis have been studied for the last four decades and are now relatively well understood, the causes and effects of landslide-generated tsunamis are much less known. The generation and effects of landslide-generated tsunamis are complex and variable. Historical landslide-generated tsunamis have produced locally extreme wave heights of hundreds of meters, as exemplified by the greater than 100-foot wave heights in Lituya Bay, Alaska, that were generated by the 1958 Lituya Bay landslide [6]. Landslide-generated tsunamis have relatively small source areas compared to the earthquake-generated tsunamis. These landslide-generated tsunamis are more prone to coastal amplification (increasing the local effect) as well as radial damping (decreasing the distal effect). This is in direct contrast to the earthquake-generated tsunamis, which are caused by elongated 2-D sources and propagate perpendicular to the source fault with little radial spreading [2, 7].

A number of researchers have investigated physical phenomena like underwater shock transport and wave motion due to landslide-and earthquake-generated tsunamis. Grilli and Watts [8] carried out 2-D, nonlinear potential flow analyses for submarine mass flow. However, due to 2-D potential flow assumption, this analysis could not account for a number of flow phenomena. Due to the assumption of 2-D potential flow, the simulations could not capture the vortex structure and viscous characteristics. Mader and Gittings [9] used the nonlinear wave equations code SWAN to simulate landslide-driven tsunamis. At Los Alamos National Laboratory, Gisler, et al. [10] used the multiphysics hydro-code SAGE to perform Navier-Stokes analysis of a hypothetical landslide. Mader and Gittings [9] used the same hydro-code [11] to simulate the submarine landslide tsunami at Lituya Bay. The last two investigations involving Navier-Stokes analysis of tsunamis were highly expensive and used hundreds of computer processing unit hours to generate meaningful results. Moreover, these analyses did not use any special surface-tracking algorithm or address the issue of flow-structure interaction. Liu, et al. [12] performed a combined experimental and numerical investigation of runup and rundown generated by three-dimensional sliding masses. They used the large eddy simulation approach in conjunction with the VOF technique to track free surface and shoreline movement.

Previous simulations of landslide-generated tsunamis can be broadly classified into two categories. In the first category, semi-empirical equations describing the center of mass motion for solid landslides [13, 8] are used, and slide kinematics is a *priori* specified in the model. This method has frequently been applied to underwater landslides, for which induced free surface waves are usually initially less complex, but some authors have also applied it to subaerial landslides [14]. In the second category, fully coupled computation of both the slide and induced fluid motion is carried out. Models based on Navier-Stokes equations have been primarily used [15, 16, 17] in these approaches. These analyses [15-17] either used (a) 2-D Navier-Stokes simulations with a VOF-type free surface tracking or (b) a multifluid finite element-based Navier-Stokes model [17] in which air and water motion were simulated. Most of the simulations were carried out in a 2-D framework; the results were quite promising, but a full three-dimensional Navier-Stokes analysis [10, 11] was computationally very expensive.

The objective of the current work is to carry out 2-D simulations of the landslide-generated tsunami at Lituya Bay, Alaska [6]. The Lituya Bay landslide-generated tsunami primarily caused a subaerial rockslide and subsequent impact into Gilbert Inlet. Triggered by an 8.3 magnitude earthquake, an estimated volume of 30.6×10^6 m^3 of amphibole and biotite schists slid down to the Gilbert Inlet at the head of Lituya Bay, causing a huge wave with a wave runup elevation of 524 m [17]. For the present simulations, the Navier-Stokes equations and the VOF method are used to track the free surface and shoreline movement. Turbulence is simulated using the RNG turbulence model [18] and the multiscale DES model [19]. Simulated results are compared with experimental data. The experiment was carried out at a 1:675 scale [20]. In the experimental setup, the subaerial rockslide impact into the Gilbert Inlet, wave generation, propagation, and runup on the headland slope were considered in a geometrically undistorted Froude similarity model. The rockslide was simulated by a granular material driven by a pneumatic acceleration mechanism so that the impact characteristics could be controlled [20].

In the current work, simulations are performed for different values of the landslide density to estimate the influence of slide density on the generated tsunami characteristics. Simulated results show the complex flow patterns in terms of the velocity field, shoreline

evolution, and free surface profiles. The predicted wave runup height is in close agreement with both the observed wave runup height and that obtained from the scaled-down experimental model [20].

2. SOLVER METHODOLOGY

FLOW-3D [21], developed by Flow Sciences, is a general purpose computational fluid dynamics simulation software package developed at Los Alamos National Laboratory in the 1960s and 1970s [22, 23, 24]. The basis of the solver is a finite volume or finite difference formulation, in an Eulerian framework, of the equations describing the conservation of mass, momentum, and energy in a fluid. The code can simulate two-fluid problems, incompressible and compressible flow, and laminar and turbulent flows. The code has many auxiliary models for simulating phase change, non-Newtonian fluids, noninertial reference frames, porous media flows, surface tension effects, and thermo-elastic behavior.

FLOW-3D solves the fully three-dimensional transient Navier-Stokes equations using the Fractional Area/Volume Obstacle Representation (FAVOR) [25] and the VOF [22] method. The solver uses finite difference or finite volume approximation to discretize the computational domain. Most of the terms in the equations are evaluated using the current time-level values of the local variables in an explicit fashion, though a number of implicit options are available. The pressure and velocity are coupled implicitly by using the time-advanced pressures in the momentum equations and the time-advanced velocities in the continuity equations. It employs an iterative method to solve these semi-implicit equations using relaxation techniques.

FAVOR [25] allows for the definition of solid boundaries within the Eulerian grid and determines fractions of areas and volumes (open to flow) in partially blocked volumes, to compute flows correspondent to those boundaries. In this way, boundaries and obstacles are defined independently of grid generation, avoiding sawtooth representation or the use of body-fitted grids. Three-dimensional solid objects are modeled as collections of blocked volumes and surfaces.

FLOW-3D has a variety of turbulence models for simulating turbulent flows. These include the Prandtl mixing length model, one- and two-equation k-ε model, RNG scheme, and a large eddy simulation model. FLOW-3D model formulation accounts for the influence of the fractional areas/volumes of the FAVOR method. In all these models, the turbulence production (or decay) associated with buoyancy forces has been formulated in a more general way. For the current simulations, the RNG model [18] is used and a multiscale DES model [19] is implemented in FLOW-3D.

3. RNG TURBULENCE MODEL

The RNG turbulence model uses statistical models to solve for the turbulent kinetic energy (k) and the turbulent kinetic energy dissipation rate (ε). The RNG-based models rely less on empirical constants while setting a framework to derive a range of parameters to be used at different turbulence scales. The RNG models use equations similar to the equations for the k-ε model. However, equation constants that are found empirically in the standard k-ε model are derived explicitly in the RNG model. Generally, the model has wider applicability than the standard k-ε model.

4. DES MULTISCALE TURBULENCE MODEL

The DES modeling approach differs from the Reynolds Averaged Navier-Stokes (RANS) modeling approach by the eddy diffusivity closure. While the RANS closure models consider the entire spectrum of turbulence, the DES variants allow some of the turbulence to be resolved explicitly, reducing the dependence on modeling. The DES formulations allow the reduction of eddy viscosity in the regions of interest, and fine scales are resolved. A switching function is used to activate the reduction in eddy viscosity. For the present simulations, a k-ε-based DES multiscale turbulence model [26] is implemented in FLOW-3D. In the DES model used, the switching function depends on both the local grid length as well as the turbulent length scale.

5. EXPERIMENT

Fritz, et al. [20] analyzed the Lituya Bay landslide-generated tsunami using a physical model. In this experimental a cross-section of the Gilbert Inlet was rebuilt at 1:675 scale in a 2-D physical laboratory model. Figure 1 shows the Gilbert Inlet illustration with the rockslide dimensions, impact site, and wave runup [20]. The Gilbert Inlet was reproduced in a rectangular prismatic channel with dimensions based on undistorted Froude similarity [17]. Figure 2 shows the simplified geometry of the Gilbert Inlet, which is the basis for the physical

experiment [20] and the current numerical simulations. Because of the specific topographic situation of the Gilbert Inlet, Fritz, et al. [20] considered the lateral spreading of the impulse wave triggered by the landslide as limited. Therefore, it was expected that the 2-D physical model gave a good prediction of wave and runup heights inside Gilbert Inlet. A novel pneumatic landslide generator was used to generate a high-speed granular slide with controlled impact characteristics. Several sophisticated laser measurement techniques such as particle image velocimetry (PIV), laser distance sensors (LDS), and capacitance wave gages (CWG) were incorporated in the experimental setup to measure the slide shape, impact time, wave features, and sequence of instantaneous velocity fields. PIV measurements of wave runup on headland slope were conducted to complement wave and runup gage records. PIV also provided instantaneous velocity vector fields in a large area of interest and gave insight into kinematics of wave generation and runup. Figure 3 shows the experimental setup with the pneumatic installations and measurement systems.

6. COMPUTATIONAL DETAILS

An idealized 2-D slice of the Lituya Bay topography was assumed for these simulations, similar to the experiments of Fritz, et al [20]. This 2-D geometry and the computational domain are shown in Figure(s) 4a, 4b and 4c. The simulation domain extends 3,187 m roughly centered on the bay and is 1,037 m in elevation from the bottom of the bay. The grid coordinate system originates at the shoreline of the northeast headland, and the bay is assumed to have a flat bottom at a depth of 122 m. A non-uniform grid comprising a mesh of 250 × 120 cells was defined for these simulations. The computational grid in the bay area consists of 100 × 30 grids in the x and z directions, respectively. The computational grids for each of the northeast and southwest headlands are 75 × 120 grids in the x and z directions, respectively. Figure 4b shows the computational grid over the entire region while figure 4c shows the enlarged view of the computational grid at the NE headland shoreline. Note that the grid also covers the initial air space above the bay between the headlands to accommodate the waves. This feature is required in the FLOW-3D software as part of its VOF free surface tracking algorithm. The boundaries at all four surfaces of the grid were specified as no-slip walls; however, the flow domain was set up so that the fluid interacted only with the boundary that defines the bottom of the bay. The left and right boundaries are almost completely obstructed by the headland surfaces. The top surface is at a high enough elevation that no waves struck this surface.

The fluid in the bay was specified as seawater with a density of 1,035 kg/m^3. The landslide material was modeled as a two-phase mixture in accordance with the drift-flux model. Three different values of landslide material density were specified: 2,600 kg/m^3 (baseline), 2,000 kg/m^3 (low), and 3,000 kg/m^3 (high). Likewise, three different values of the initial void fraction of the landslide material were specified: 39% (baseline), 30% (low), and 50% (high). The baseline values are consistent with those Fritz, et al. [20] used in the scale experiments of the Lituya Bay incident. For these simulations, the voids in the landslide mass are filled with seawater as the software requires. This is obviously not representative of the real landslide material, but is required by the drift-flux model of the landslide-water mixture to allow the landslide to move down the headland slope as a fluid. Fritz, et al. [20] estimated the bulk density of the material as 1.61t/m^3, considering a void fraction of 39% from the data obtained on Alpine debris flow. Most of the simulations in the current work were performed under the assumption of a hydrodynamically smooth surface for the headlands; however, one simulation was performed with a rough surface model. In this case, the nominal roughness height was arbitrarily assumed to be 2 m as a reasonable representation of terrain roughness and the presence of trees. The simulations did not consider phase change for the slide material. In addition, the volume increase (and density decrease) associated with the conversion from a rock mass to a granular flow as well as dilatation of the flow was not included.

For the present simulations, the pressure-based solver was chosen along with the implicit algorithm. The viscous stress was computed using an explicit scheme. For the advection equations, an explicit scheme was used. A second-order central difference scheme was used for the momentum equations. No qualitative or quantitative difference was observed between the simulation results carried out with the RNG model and the DES model. The DES turbulence model is most suitable for 3-D flows with major separation regions. For the current configuration, the simulations were all carried out in 2-D; therefore, there was no difference between RNG

and DES model predictions. Hence, all results presented in this paper are based on the RNG turbulence model.

7. RESULTS AND DISCUSSION

Computed results are presented for the time evolution of the landslide and water phases after the landslide mass hits the bay. The computed results are compared with the experimental data. In addition, the wave record and the wave runup record at different locations are also compared with the experimental data. The effect of initial void fraction and landslide particle density on the wave runup is also presented.

Figure 5 presents the evolution of the flow-field with time as the landslide impacts the water bay. According to Fritz, et al. [20], the whole process can be subdivided into two main stages: a) slide impact and penetration, flow separation, and cavity formation (shown in Figure 5(a) and (b) cavity collapse, slide runout along the channel bottom and slide detrainment, and propagation out of the impact area. The large air cavity develops at the rear of the slide as its penetration velocity is larger than the wave velocity. As can be observed in Figure 5(d), 20 seconds after impact, the air cavity subsequently collapses during the slide runout along the bottom. The mixing of the air and water phase can be observed at this instance.

Figure 6 shows the observation from the experiment [20]: the unsteady flow and instantaneous velocity vectors offer insight into the process. Flow reattachment causes the entrapment of a large volume of air in the back of the rockslide, which leads to a large bubble formation, bubble break up, and phase mixing. Figures 5 and 6 show that the current simulations predict the sequence of events in close agreement with the experimental observation.

Figure 7 shows the sequence of wave runup on the southwest headland slope created by the rockslide impact. At 18 seconds after impact, the wave is shown prior to plunging onto the headland ramp. In the two subsequent instantaneous figures, the wave surges up the headland slope; the waterfront moves up the headland ramp with time. In addition, notice that the sheet of water located on the headland ramp is getting significantly thinner at the topmost point when the maximum runup height is reached.

Figure 8 shows the corresponding instantaneous snapshots from the experimental results; the predicted results are in close agreement with the results obtained by the experiment. However, the maximum runup at the headland predicted by the current simulations is higher than that observed in the experiment [20]. The predicted maximum runup is around 673 m compared to the 527 m runup observed in the experiment. This can be attributed to reduced energy dissipation in the numerical model and the assumption of a hydrodynamically smooth surface with very little surface roughness. Consideration of phase mixing, non-zero friction, and hydrodynamically rough surfaces may reduce the height elevation and maximum runup close to the headland. Future simulations will evaluate the effect of variable rough surface and non-zero friction on the predicted maximum runup height. Initial preliminary simulations with surface roughness showed some decrease in runup height. Preliminary results with surface roughness are presented in Figures 9 and 11.

Figure 9 shows the predicted wave record at location x = 885 m for the simulations with different void fractions. The wave propagating away from the impact area in the positive x direction creates a peak at t ~ 20 sec with maximum positive amplitude of 200 m. The single outward traveling wave is reflected back and forth from both headland and rockslide ramps. The second peak on the curve corresponds to the wave reflection from the headland propagating in the negative x direction. The subsequent peaks can be attributed to partial back and forth wave reflection. The reflections take place from the rockslide slope and from the headland ramp, respectively. Also note that the wave heights in the bay are affected differently by the changes in the density of the landslide mass. The initial wave created by the landslide in the bay is not significantly affected by the landslide material density. The heights of succeeding waves, however, are generally proportional to the landslide density regardless of whether the density change is a result of changing the particle density or void fraction. Note that the surface roughness has little effect on the wave heights in the bay.

Figure 10 shows the corresponding experimental results. The simulations predict the wave height in good qualitative agreement with the experimental results. Among the different cases, the case with 39% initial void fraction and surface roughness provides the closest agreement with the experiment.

Figure 11 shows the predicted wave runup record on the headland ramp at x = 1,342 m for the different cases. Among the different cases, the simulation case with 39% void fraction and

rough surface predicts a maximum runup height of 627 m on the headland ramp. All other cases predict a much higher runup. The measured highest runup height as seen from Figure 12 is 526 m. The observed highest elevation at the Gilbert Inlet was 524 m. [6]. Figure 11 also shows that the initial run up on the SW headland is only slightly affected by the landslide density. However, the presence of headland roughness reduces the wave runup on the SW headland by about 25%. The two trailing peaks on the runup correspond to the multiple reflections of the single initial wave runup. Comparing Figures 11 and 12 shows that the predictions are in good qualitative agreement with the experimental observations. Simulations by Schwaiger, et al. [1] found that increasing the rockslide viscosity significantly reduces the runup height.

8. CONCLUSIONS

Numerical simulations were conducted to assess the impulse waves generated by the subaerial landslide at Lituya Bay, Alaska. The VOF method is used to track the free surface and shoreline movements. The simulation results are compared with experimental results obtained in a physical model of a real case. The numerical results obtained from the simulations are in good agreement with the measured experimental results. Computed results show that the model captures the basic flow features associated with the time-dependent evolution of the flowfield as the landslide interacts with the bay. The choice of DES and RNS turbulence models does not affect the simulation results. The wave characteristics are found to be only slightly dependent on the void fraction and slide material density. The predicted maximum runup was overpredicted compared to the experimental results. This was due to the assumption of almost hydrodynamically smooth surface and small surface roughness. The evolution of the flowfield and the runup is significantly influenced by the slide theology, surface roughness, and energy dissipation. The value of the slide viscosity effectively incorporates both the dissipation of energy through deformation as well as the energy lost through turbulence in the impact process. Further simulations will be carried out to analyze the effect of the slide rheology on the predicted runup and the mechanism of energy dissipation.

9. ACKNOWLEDGMENTS

This work was sponsored by the Advisory Committee for Research at Southwest Research Institute® through an Internal Research and Development Project. The authors acknowledge the useful discussions provided by the technical support staff at FlowSciences, Inc.

10. REFERENCES

1. Schwaiger, H. F., and Higman, B., 2008, "Lagrangian hydrocode simulations of the 1958 Lituya Bay tsunamigenic rockslide," Geochemistry, Geophysics, Geosystems, 8(7), Q07006.10.1029/2007GC00154.
2. Masson, D. G., Harbitz, C. B., Wynn, R. B., Pedersen, G., and Lovholt, F., 2006, "Submarine Landslides: Processes, Triggers and Hazard Prediction," Philosophical Transaction of the Royal Society, Vol. 364, pp. 2009–2039.
3. Longva, O., Janbu, N., Blikra, L. H. and Boe, R., 2003, "The Finneidfjord Slide: Seafloor Failure and Slide Dynamics," Submarine Mass Movements and Their Consequences, J. Locat and J. Mienert, eds., Kluwer Academic Publishers, Dordrecht, Netherlands, pp. 531–538.
4. Fine, I. V., Rabinovich, A. B., Bornhold, B. D., Thomson, R. E., and Kulikov, E. A., 2005, "The Grand Banks Landslide-Generated Tsunami of November 18, 1929: Preliminary Analysis and Numerical Modeling," Marine Geology, Vol. 203, pp. 201–218.
5. Piper, D. J. W., Cochonat, P., and Morrison, M. L., 1999, "The Sequence of Events Around the Epicenter of the 1929 Grand Banks Earthquake: Initiation of Debris Flows and Turbidity Currents Inferred From Sidescan Sonar," Sedimentology, Vol. 46, pp. 79–97.
6. Miller, D. J., 1960, "Giant waves in Lituya Bay, Alaska," Geological Survey Professional Paper 354-C, U.S. Government Printing Office, Washington, DC.
7. Harbitz, C. B., Lovholt, F., Pederson, G., and Masson, D.G., 2006, "Mechanisms of Tsunami Generation by Submarine Landslides: A Short Review," Norwegian Journal of Geology, Vol. 86, pp. 255–264.
8. Grilli, S. T., and Watts, P., 2005, "Tsunami Generation by Submarine Mass Failure, I: Modeling, Experimental Validation, and Sensitivity Analysis," Journal of Waterway, Port, Coastal, and Ocean Engineering, Vol. 131, pp. 283–297.
9. Mader, C. L., and Gittings, M. L., 2002, "Modeling the 1958 Lituya Bay Mega Tsunami-II," Science of Tsunami Hazards, 20(4), pp. 241–355.

10. Gisler, G., Weaver, R., Mader, C., and Gittings, M. L., 2003, "Two- and Three-Dimensional Simulations of Asteroid Ocean Impacts," Science of Tsunami Hazards, 21(2), pp. 119–134.
11. Gisler, G., Weaver, R., and Gittings. M. L., 2006, "SAGE Calculations of the Tsunami Threat From La Palma," Science of Tsunami Hazards, 24(4), pp. 288–312.
12. Liu, P. L. -F., Wu, T. -R., Raichlen, F., Synolakis, C. E., and Borrero, J. C., 2005, "Runup and Rundown Generated by Three-Dimensional Sliding Masses." Journal of Fluid Mechanics, Vol. 536, pp. 107–144.
13. Grilli, S. T., and Watts, P., 1999, "Modeling of Waves Generated by a Moving Submerged Body, Applications to Underwater Landslides," Engineering Analysis with Boundary Elements, Vol. 23, pp. 645–656.
14. Lynett, P. and Liu, P. L. -F., 2005, "A Numerical Study of the Runup Generated by Three-Dimensional Landslides," Journal of Geophysical Research, 110(C03006), doi:10.1029/2004JC002443.
15. Rzadkiewicz, A. S., Mariotti, C., and Heinrich, P., 1997, "Numerical Simulation of Submarine Landslides and Their Hydraulic Effects," Journal of Waterway, Port, Coastal, and Ocean Engineering, 123(4), pp. 149–157.
16. Heinrich, P., 1992, "Nonlinear Water Waves Generated by Submarine and Aerial Landslides," Journal of Waterway, Port, Coastal, and Ocean Engineering, 118(3), pp. 249–266.
17. Quecedo, M., Pastor, M.,and Herreros, M. I., 2004, "Numerical Modeling of Impulse Wave Generated by Fast Landslides," International Journal for Numerical Methods in Engineering, Vol. 59, pp. 1633–1656.
18. Yakhot, V., and Smith, L. M., 1992, "The Renormalization Group, the e-Expansion and Derivation of Turbulence Models," Journal of Scientific Computing, Vol. 7, pp. 35–61.
19. Basu, D., 2006, "Hybrid Methodologies for Multiscale Separated Turbulent Flow Simulations," PhD. Dissertation, University of Cincinnati.
20. Fritz, H. M., Hager, W. H., and Minor, H. E., 2001, "Lituya Bay Case: Rockslide Impact and Wave Run-up," Science of Tsunami Hazards, 19(1), pp. 3–22.
21. Flow Sciences Incorporated, 2006, "Flow3D Users Manual Version-9.1," Publisher, Santa Fe, New Mexico.
22. Hirt, C. W., and Nichols, B. D., 1981, "Volume of Fluid (VOF) Method for the Dynamics of Free Boundaries," Journal of Computational Physics, Vol. 39, pp. 201–225.
23. Harlow, F. H., and Welch, J. E., 1965, "Numerical Calculation of Time-Dependent Viscous Incompressible Flow," Physics of Fluids, Vol. 8, pp. 2182–2189.
24. Welch, J. E., Harlow, F. H., Shannon, J. P., and Daly, B. J., 1966, "The MAC Method: A Computing Technique for Solving Viscous, Incompressible, Transient Fluid Flow Problems Involving Free-surfaces," Los Alamos Scientific Laboratory report LA-3425.
25. Hirt, C. W., and Sicilian, J. M., 1985, "A Porosity Technique for the Definition of Obstacles in Rectangular Cell Meshes," Proceedings of the Fourth International Conference on Ship Hydrodynamics, National Academy of Sciences, Washington, DC, pp. 1–19.
26. Basu, D., Hamed, A., Das, K., Tomko, K. and Liu, Q., 2006, "Comparative Analysis of Hybrid Turbulence Closure Models in Unsteady Transonic Separated Flow Simulations," AIAA-2006-0117.

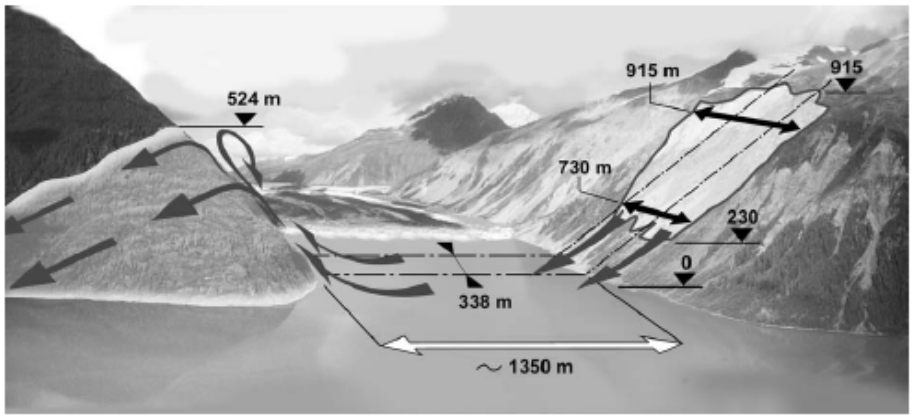

Figure 1. Illustration of Gilbert Inlet showing the dimensions of the rockslide, dimensions of the impact site, and wave runup (Photo courtesy of Hermann M. Fritz and Charles L. Mader: Fritz, et al. [20])

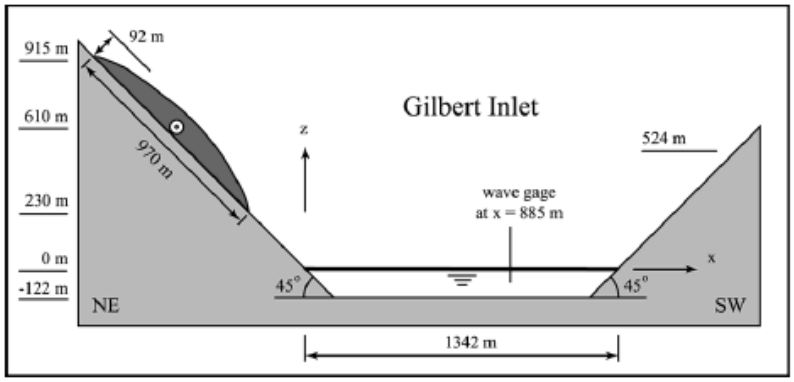

Figure 2. Simplified geometry of the Gilbert Inlet, the basis of the physical and numerical model used in the simulations (from Fritz, et al. [20])

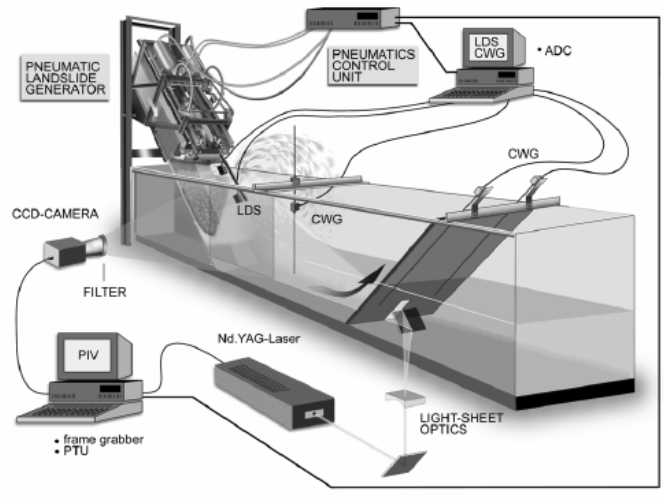

Figure 3. Experimental setup with pneumatic installation and measurement systems such as LDS, CWG, and PIV (from Fritz, et al. [20])

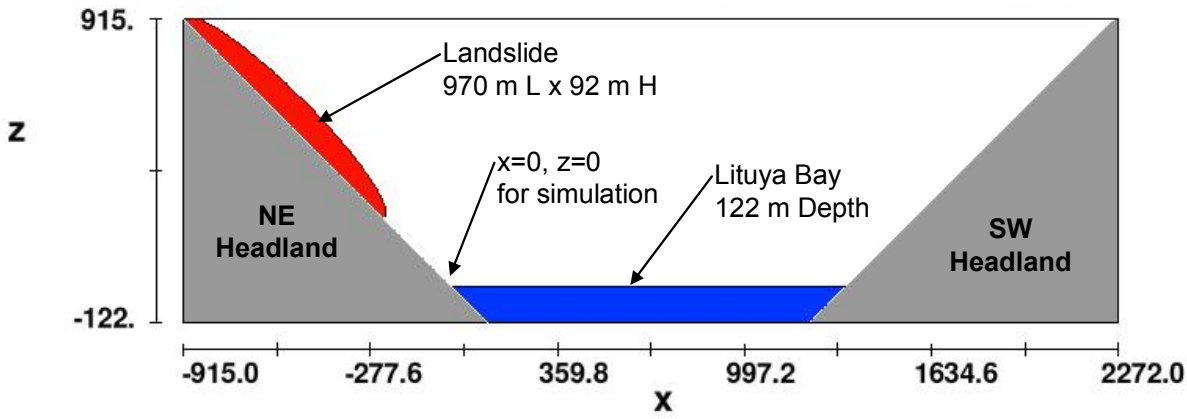

Figure 4a. Geometry and computational domain for the Gilbert Inlet

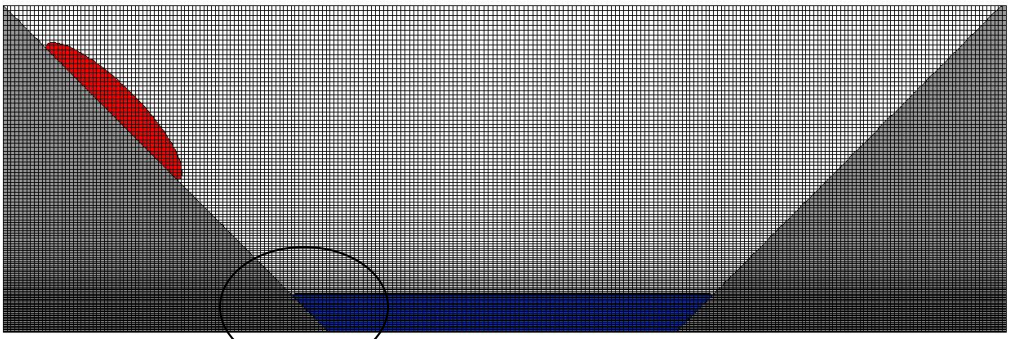

Figure 4b Computational grid for the Gilbert Inlet

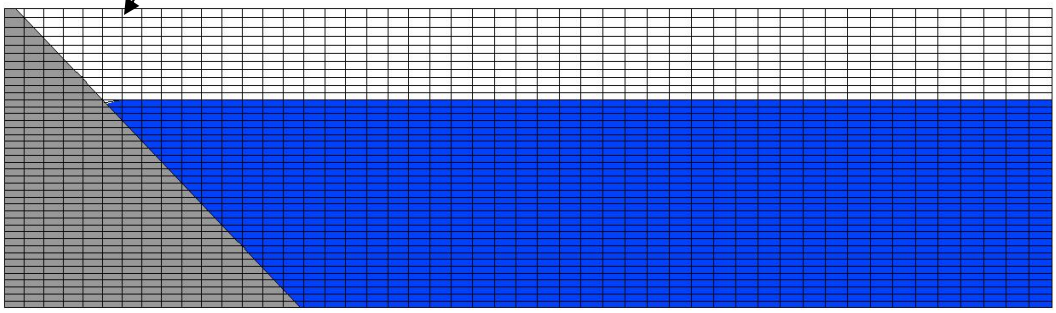

Figure 4c Detailed view of the computational mesh at the NE headland shoreline

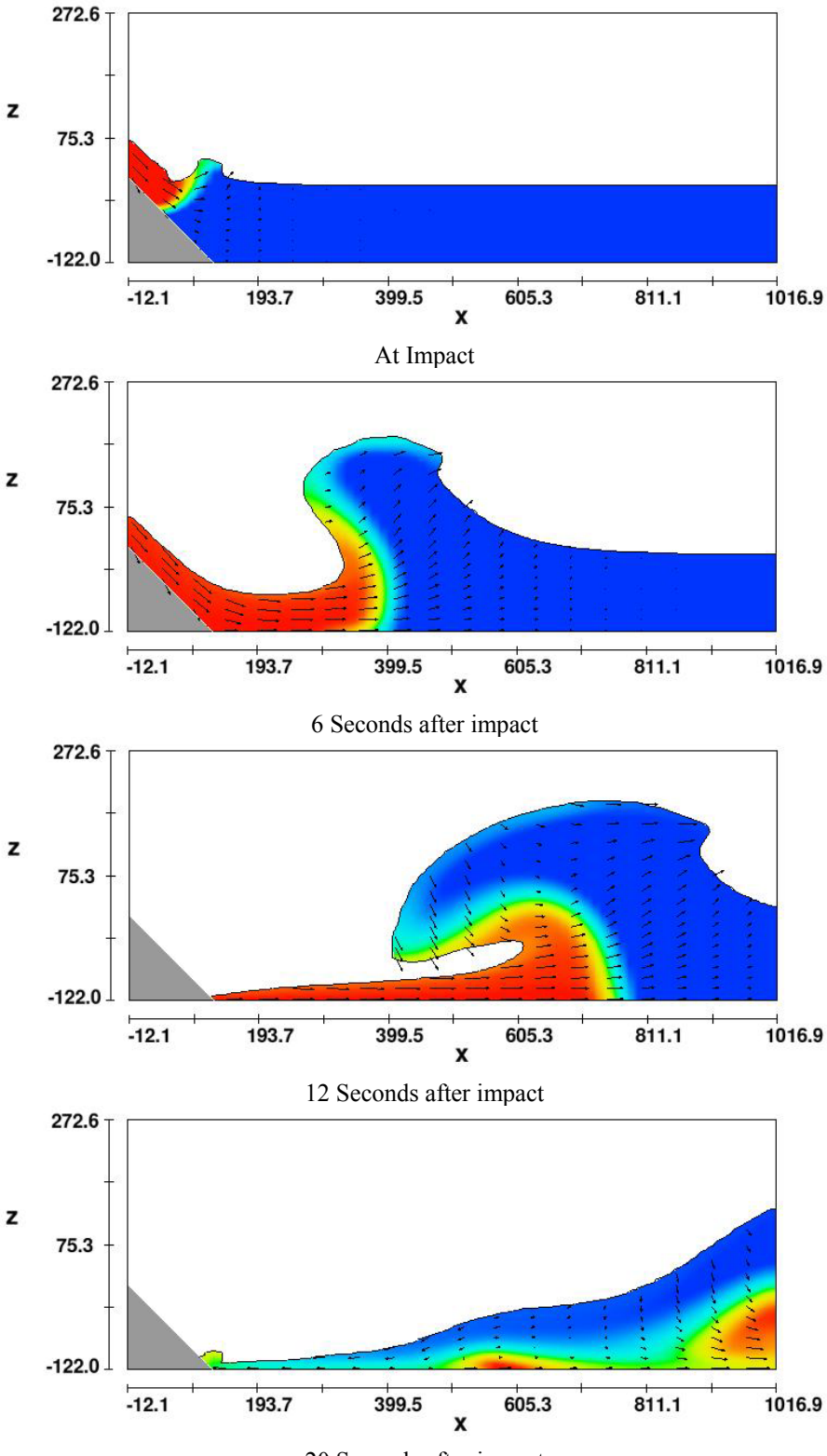

Figure 5. Evolution of the flowfield after landslide impact with time (computational results)

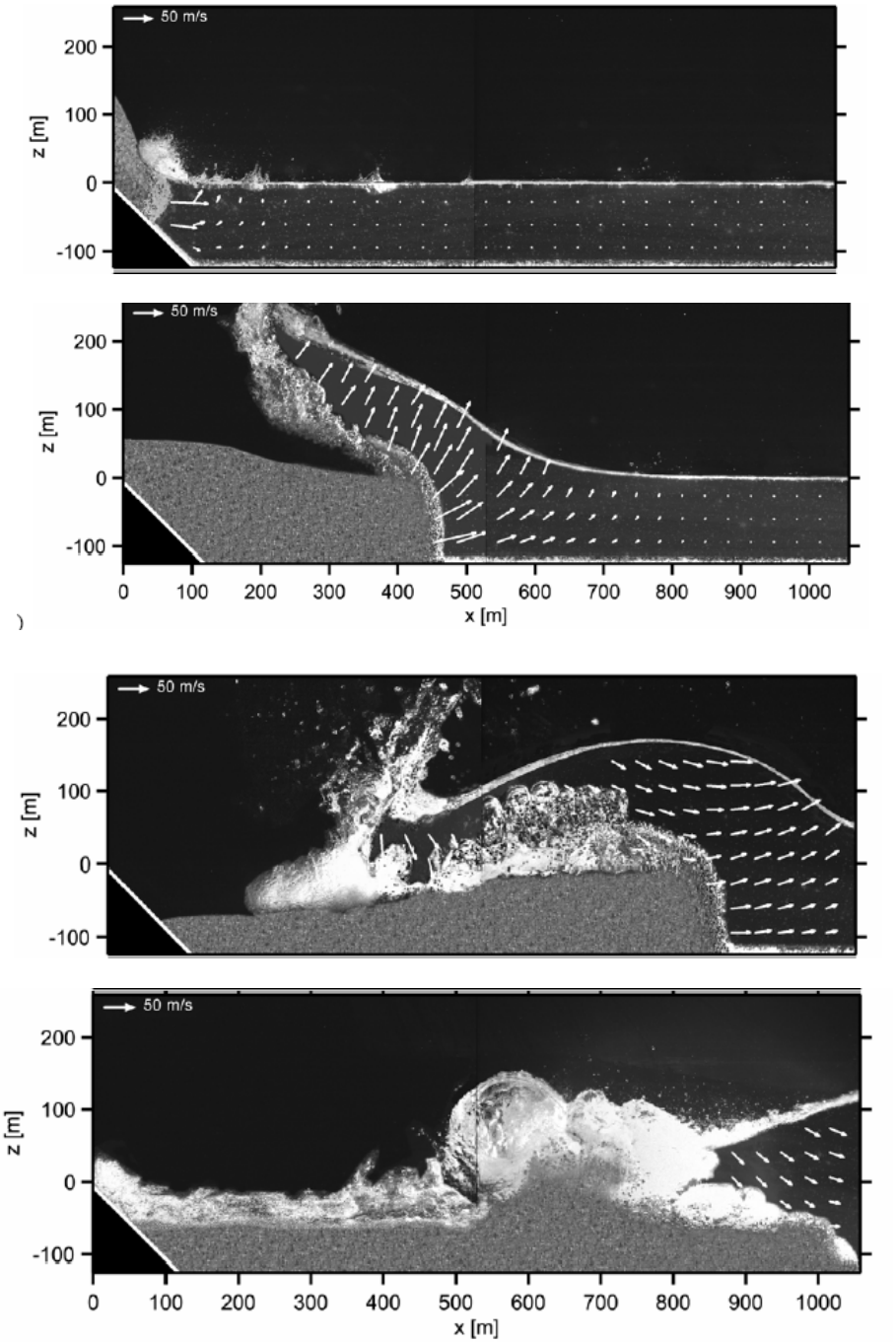

Figure 6. Evolution of the flowfield after landslide impact with time (experimental results) [PIV velocity vector field sequence] (from Fritz, et al. [20])

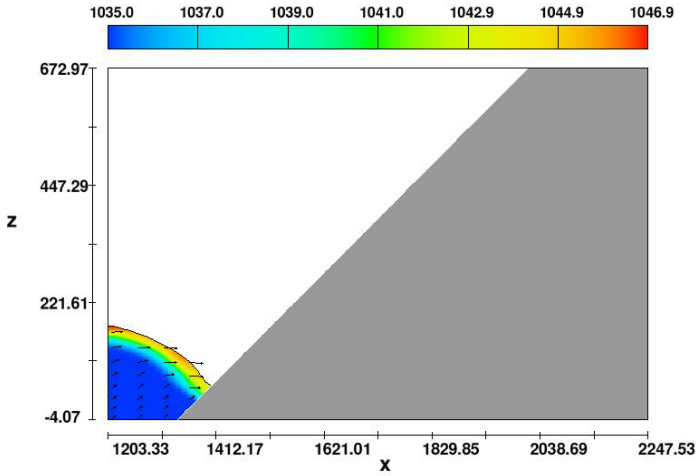

18 Seconds after impact

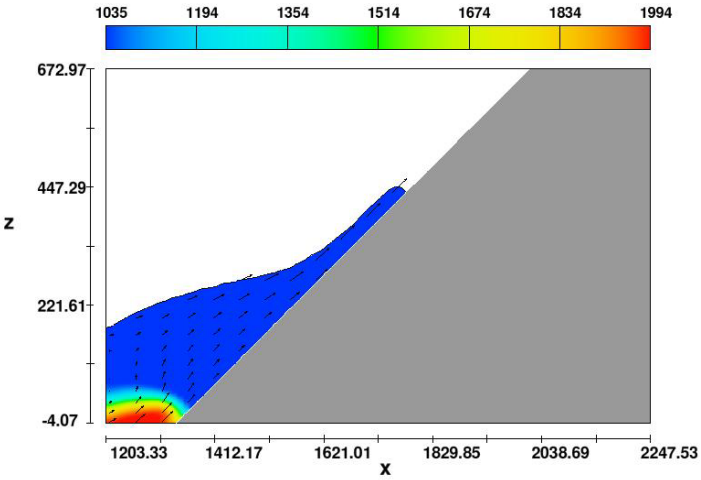

24 seconds after impact

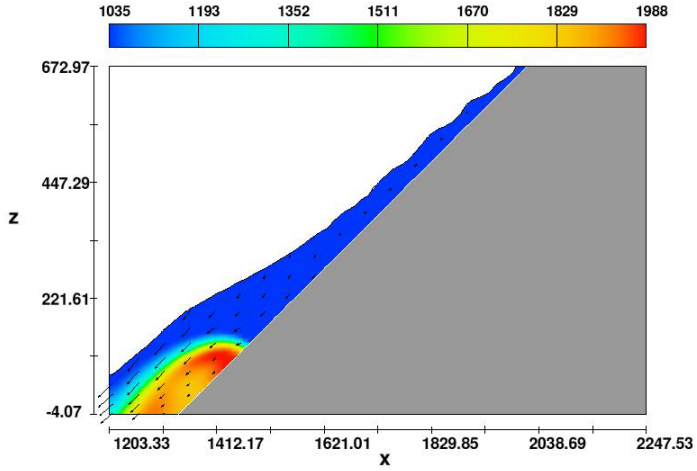

34 seconds after impact

Figure 7. Evolution of the flowfield with wave runup sequence on headland slope (computational results)

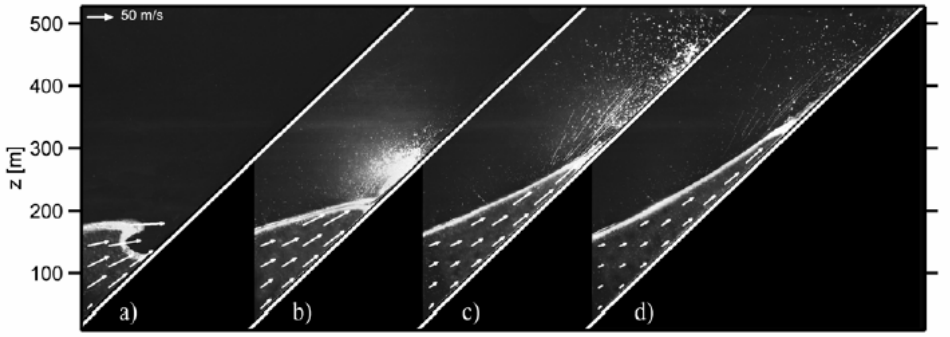

Figure 8. PIV velocity vector-field sequence of wave runup on headland slope (experimental results) (from Fritz, et al. [20])

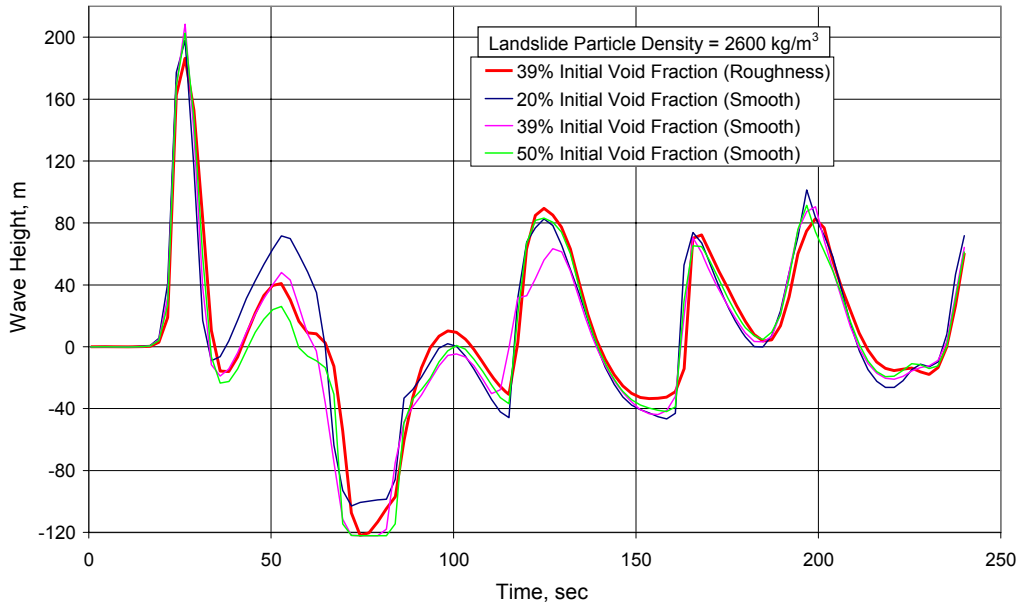

Figure 9. Predicted wave height record at location x = 885 m for different values of initial void fraction

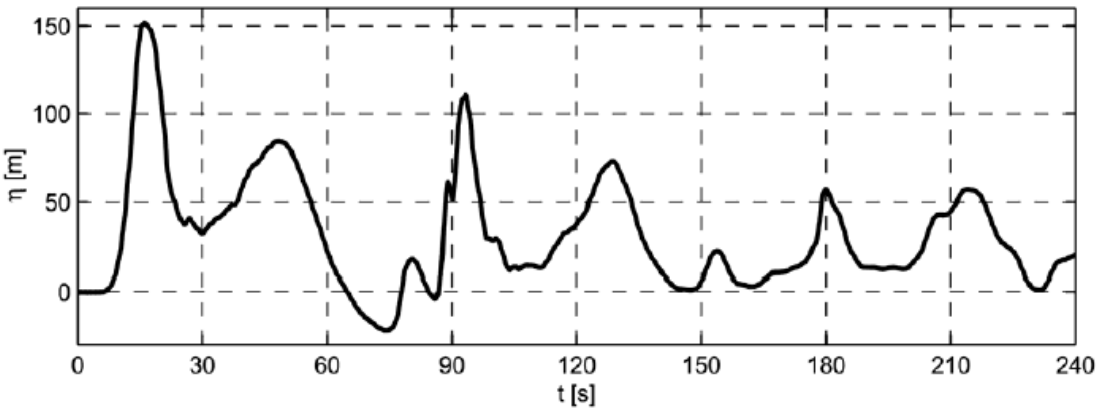

Figure 10. Wave record at location x = 885 m (experimental results) (from Fritz, et al. [20])

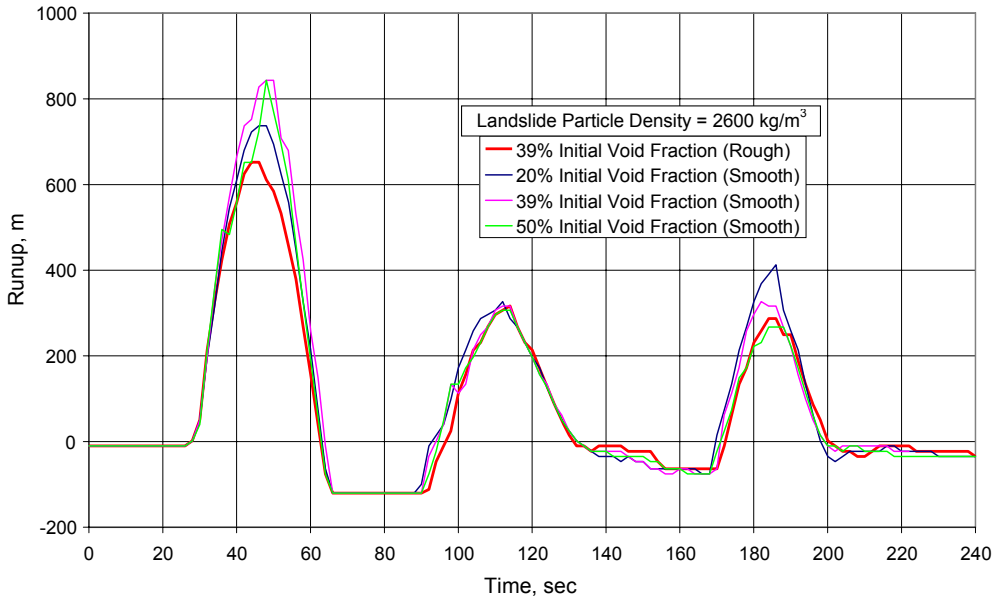

Figure 11. Predicted wave runup record on headland ramp at locations x = 1,342 m

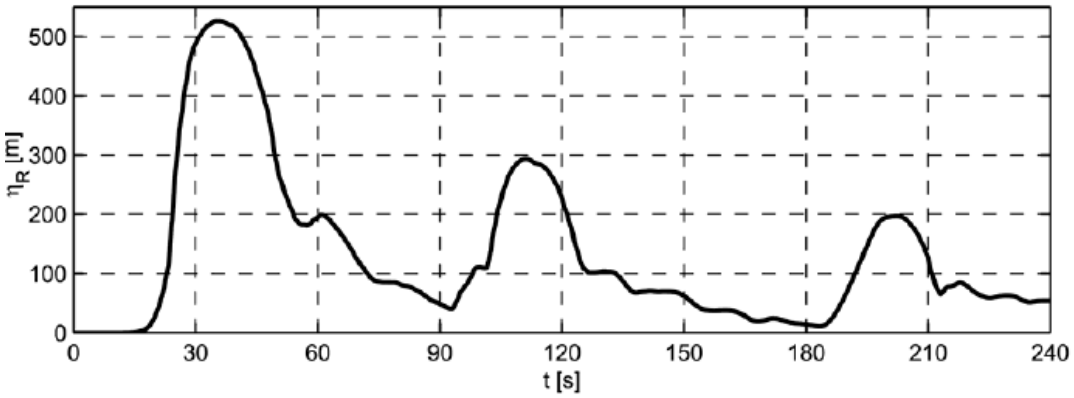

Figure 12. Experimental observation of wave runup record on headland ramp at locations x = 1,342 m (from Fritz, et al. [20])